ADVANCED MATERIALS
www.advmat.de

Check for updates

Self-Powered MXene/GaN van der Waals Heterojunction Ultraviolet Photodiodes with Superhigh Efficiency and Stable Current Outputs

*Weidong Song, Jiaxin Chen, Ziliang Li, and Xiaosheng Fang**

A self-powered, high-performance $Ti_3C_2T_x$ MXene/GaN van der Waals heterojunction (vdWH)-based ultraviolet (UV) photodiode is reported. Such integration creates a Schottky junction depth that is larger than the UV absorption depth to sufficiently separate the photoinduced electron/hole pairs, boosting the peak internal quantum efficiency over the unity and the external quantum efficiency over 99% under weak UV light without bias. The proposed $Ti_3C_2T_x$/GaN vdWH UV photodiode demonstrates pronounced photoelectric performances working in self-powered mode, including a large responsivity (284 mA W^{-1}), a high specific detectivity (7.06×10^{13} Jones), and fast response speed (rise/decay time of 7.55 µs/1.67 ms). Furthermore, the remarkable photovoltaic behavior leads to an impressive power conversion efficiency of 7.33% under 355 nm UV light illumination. Additionally, this work presents an easy-processing spray-deposition route for the fabrication of large-area UV photodiode arrays that exhibit highly uniform cell-to-cell performance. The MXene/GaN photodiode arrays with high-efficiency and self-powered ability show high potential for many applications, such as energy-saving communication, imaging, and sensing networks.

1. Introduction

UV photodetectors (PDs) are fundamental optoelectronics components with ability to convert incident short-wavelength (<400 nm) radiation into electrical signals for further processing. Based on capturing, identifying, and visualizing optical information, UV PDs have a wide range of applications in many areas, such as secure communication, imaging, biological detection, chemical analysis, and daily life monitoring, etc.[1–3] For decades, commercial UV PDs are mainly established on the vacuum photomultipliers and the UV-enhanced Si photodiodes. However, vacuum devices meet many issues, such as large volume, high operating voltage, and especially their fragile essence when a vacuum tube is used.[4] Si-based UV devices are inborn with narrow and indirect bandgap which limits UV light absorption, resulting in low quantum efficiency. Moreover, the fabrication of high-performance Si photodiodes (e.g., p–n or p–i–n junctions) usually suffers from complex microfabrication processes, such as high-temperature diffusion and ion implantation, leading to the reduction of minority carrier lifetime and the great degradation of photoelectric performances.[5]

Lasting for decades, great efforts made in searching for novel materials and device configurations are still ongoing for high-performance UV PDs, in order to meet the requirements in the modern miniaturized electronic industry. Benefiting from several advantages, such as the strong light–matter interaction, thickness-dependent bandgap, high in-plane carrier mobility, and sound transparency, 2D materials (2DMs) or layered materials have been proved to be one of the best material candidates for the construction of PDs working at different response spectrum.[6,7] Recently, a series of wide-bandgap semiconducting (i.e., with bandgap > 3.0 eV) 2DMs, for example, $Ga_2In_4S_9$,[8] $NiPS_3$,[9] BiOBr(I),[10,11] perovskite $Sr_2Nb_3O_{10}$,[12] has emerged as efficient materials for UV PD applications. Nevertheless, a further enhancement of the photoelectric performances of the 2DMs is still of great challenge due to their small photoresponsivity and low on/off ratio induced by the low light absorption though intriguing electronic and optical attributes of the thin layers.[13] Alternatively, the construction of a van der Waals heterojunction (vdWH) platform shows high prospect for enhanced photoelectric performances.[14] Dangling-bond-free surfaces of 2DMs and layered materials break the strict restriction of lattice matching, making them possible for high-quality vdWHs integrated on arbitrary mature bulk semiconductors, such as Si, Ge, GaAs, GaN, etc.[15–18] Such systems may trigger new coupling phenomena between 3D bulk materials and 2DMs/layered materials.[19] Thanks to the great optical absorption of the 3D bulk films and the local electrical field introduced by vdWHs, the photoinduced electron/hole pairs can be effectively separated, pointing toward highly efficient photo-to-electric conversion. In addition, the integration of 2DMs/layered materials with 3D bulks is of high compatibility

Dr. W. D. Song, Dr. J. X. Chen, Dr. Z. L. Li, Prof. X. S. Fang
Department of Materials Science
Fudan University
Shanghai 200433, P. R. China
E-mail: xshfang@fudan.edu.cn
Dr. W. D. Song
College of Applied Physics and Materials
Wuyi University
Jiangmen 529020, P. R. China
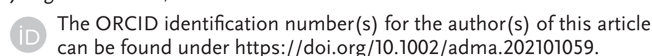
The ORCID identification number(s) for the author(s) of this article can be found under https://doi.org/10.1002/adma.202101059.

DOI: 10.1002/adma.202101059

 © 2021 Wiley-VCH GmbH

with the currently mature planar microfabrication process, providing a broad avenue for future large-scale production and application.[20]

As a new branch of layered materials, MXenes exhibit fascinating electronic and optical properties, rendering them a wide range of (opto)electronic applications such as transistors,[21] capacitors,[22] solar cells,[23] light-emitting diodes,[24] lasers and PDs,[17,25] etc. MXenes refer to layered transition-metal carbides, nitrides, or carbon-nitrides, such as Ti_3C_2, MoC_2, V_3C_2, Ti_4N_3, which are produced by exfoliation MAX phase.[26] Extraordinarily, the intriguing surface functionality of MXenes enables them to artificially engineer work functions (WFs) and electronic band structures, providing additional regulatory pathway for optoelectronics.[27] The tunable WFs (from 1.6 to 8.0 eV)[28] together with their metallic conductivity and good optical transmittance, MXenes are considered as excellent Schottky electrode materials beyond Au.[17] To date, MXenes have been integrated with Si,[29] GaAs,[17] TiO_2,[30] perovskite,[31] etc. for photodetection, where they serve as transparent Schottky contacts. Among 3D bulk materials, GaN, as a member of the third-generation semiconductors, has been developed as an excellent candidate for UV photodetection due to its direct wide-bandgap of 3.4 eV, excellent radiation hardness, and high thermal conductivity.[32–34] However, the integration of MXene and GaN that may bring about intriguing attributes has not been explored yet for UV optoelectronics.

Here, we demonstrate the MXene/GaN vdWH photodiodes for UV light detection. The as-prepared $Ti_3C_2T_x$/GaN vdWH UV photodiodes exhibit superhigh internal quantum efficiency (IQE) exceeding 100% and the peak external quantum efficiency (EQE) surpassing 99% (355 nm, 30 μW cm^{-2}) when working in the self-powered mode. To the best of our knowledge, these are champion merits for a UV PD without external power supply. This remarkable enhancement is attributed to the high Schottky barrier formed between $Ti_3C_2T_x$ and GaN that can effectively separate photogenerated carriers, which is confirmed by the scanning Kelvin probe force microscopy (SKPFM) measurements. Simultaneously, the UV light absorption of MXene induces hot carriers that further contribute to the photocurrents. Moreover, the UV photodiode shows fast response speed (rise/decay time of 7.55 μs/1.67 ms) and a remarkable specific detectivity of 7.06×10^{13} Jones. Especially, the pronounced photovoltaic behavior gives rise to a high power conversion efficiency (PCE) of 7.33% under 355 nm UV illumination. In addition, the simple spray depositing method allows for fabricating large-area MXene/GaN photodiode arrays with high uniformity, providing high possibility for the further design of practical applications.

2. Results and Discussion

Figure 1a,b schematically displays the preparation process of the $Ti_3C_2T_x$ colloidal solution and the $Ti_3C_2T_x$ film/GaN vdWHs. Starting from the chemically etched $Ti_3C_2T_x$ MXene solution prepared by removing Al atoms from Ti_3AlC_2 MAX phase, a centrifugation and subsequent manual shaking process have been conducted to delaminate the MXene into layered flakes. The $Ti_3C_2T_x$ flakes show thickness distribution ranging from 2 to 7 nm, which is determined by the atomic force microscopy (AFM) (Figure S1, Supporting Information), supporting their few-layered structures.[35] The obtained MXene colloidal suspension was then deposited on GaN through a spray coating method conducted in ambient air. To define the contact area, different masks were used, resulting in MXene/GaN vdWHs arrays, as shown in Figure 1c. The surface morphologies of the as-deposited MXene film and GaN were observed by scanning electron microscopy (SEM), as shown in Figure 1d,e and Figure S2, Supporting Information. It is clear that the surface of the GaN film is uniformly covered by MXene flakes with the emergency of some wrinkles. The stacked $Ti_3C_2T_x$ flakes collectively form the compactly packed film with a height variation of ≈12 nm at the MXene/GaN edges (Figure 1f). X-ray diffraction (XRD) and Raman experiments were carried out to characterize the as-deposited MXene flake films (Figure 1g,h). The XRD peak centered at $2\theta = 9.5°$ corresponding to (002) planes of Ti_3AlC_2 MAX phase is set as a reference.[26] The XRD patterns of the $Ti_3C_2T_x$ exhibit a blueshifted 2θ angle (≈7.3°) compared to that of the Ti_3AlC_2 MAX, which further confirms the successful exfoliation of the few-layered $Ti_3C_2T_x$ MXene and the existence of surface terminated functionalities and water molecules between MXene layers.[36,37] The broad peaks in the Raman spectra are also supposed to be related to the coexistence of various surface terminated functional groups.[38] It is noteworthy that the peaks at ≈150 cm^{-1}, which corresponds to the TiO_2 not being observed.

The reflectance spectra of MXene/GaN with different MXene film thicknesses are given in Figure 1i. The thickness of the sprayed MXene film was controlled via a fine control of the spraying amount of $Ti_3C_2T_x$ MXene solution, ranging from 1 to 4 mL, henceforth referred as SP1 to SP4. The pure GaN exhibits a cut-off at ≈364 nm which corresponds to its optical bandgap of 3.4 eV. When increasing the MXene film thickness, distinct reflectance properties are observed for phonon energy above and below E_g of GaN. In detail, the reflectance shows a positive correlation with the MXene film thickness when the wavelength range is shorter than the cut-off, whereas a negative relationship for that longer than the cut-off wavelength. Figure S3, Supporting Information shows the transmittance spectra of MXene film on quartz with different thicknesses and the insets display their digital pictures. It shows that more than 80% of near-UV light can penetrate through the thin enough MXene film, taking the SP2 sample at 355 nm as an example. In fact, both the absorption of MXene and GaN contribute to the total UV-generated photocurrent in the Mxene/GaN UV photodiode, resulting in an ultrahigh IQE over 100%, as will be detailed below.

Figure 2a schematically presents the device structure of the MXene/GaN vdWH photodiode. To make the devices, InGa eutectic ohmic electrode was made on GaN side (Figure S4, Supporting Information). Figure 2b displays typical current–voltage (*I–V*) curves of the SP2 photodiode in the dark and under three UV light illuminations (250, 300, 355 nm). Rectification characteristics are obviously observed when the *I–V* curves presented in linear scale (see Figure S5a, Supporting Information), which is originated from the Schottky barrier formed at the metallic MXene/GaN interface that dominates the current transport. The vdWH photodiode has a low dark current under 0 V and reverse bias (I_{dark} of 3.28 pA at 0 V and 14 pA at –1 V), which is

 © 2021 Wiley-VCH GmbH

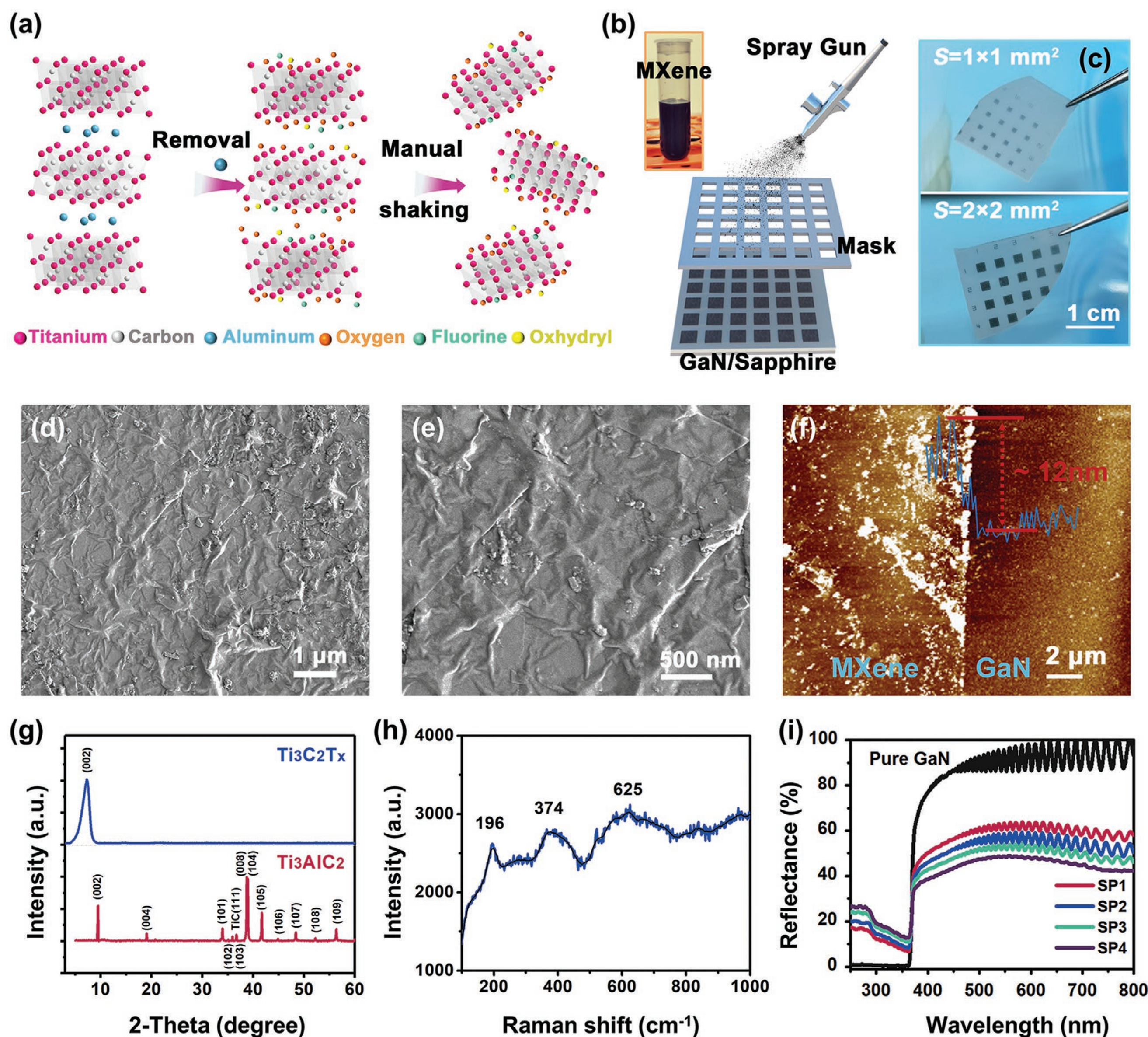

Figure 1. a,b) Schematic illustration of the preparation of Ti_3C_2-based MXene colloidal suspension and the deposition of MXene onto GaN via the spray-deposition method using a mask to define the contacting area. The inset digital photograph shows the as-prepared MXene colloidal suspension. c) Digital photograph of typical 1 × 1 and 2 × 2 mm^2 square MXene electrode arrays on GaN. d–f) SEM and AFM images showing surface and interface between sprayed MXene film and GaN. g) XRD patterns of the as-sprayed MXene flakes film, where the patterns of Ti_3AlC_2 MAX are referenced. h) Raman spectra of the $Ti_3C_2T_x$ MXene. i) The reflectance spectra of the GaN before and after spray coating MXene with different thicknesses.

remarkably smaller than that of Au/GaN Schottky photodiode (I_{dark} of 42 pA at 0 V and 352 pA at –1 V, Figure S6, Supporting Information) with the same active area of 4 mm^2. This is probably related to the finite density of states within $Ti_3C_2T_x$ when compared to metal/semiconductor contacts.[39] Moreover, the time-dependent I_{dark} both at 0 V and reverse bias are highly durable within the measured time domain, which confirms the establishment of high-quality and robust vdWH (Figure S5b, Supporting Information). More than six, five, and four orders of magnitude current enhancements are achieved for the light illumination with wavelength of 355, 300, and 250 nm at 0 V. The photocurrent reaches saturation at 0 V bias, manifesting strong enough built-in electrical field at 0 V bias to efficiently separate photoinduced carriers. The photovoltaic behavior suggests that the vdWH photodiode is capable of operating in both self-bias and zero-bias modes. In the following text, photoresponse properties and performances of the MXene/GaN vdWH photodiode are rated at 0 V bias, unless otherwise stated.

Photo-to-dark current ratio I_{light}/I_{dark} at the three measured UV wavelengths as a function of spray amount of $Ti_3C_2T_x$ solution is deduced and shown in Figure 2c. The SP2 photodiode exhibits a superhigh I_{light}/I_{dark} of 1.42×10^6 at 355 nm, showing an outstanding signal-to-noise ratio. This is the origin of the large photocurrent and extremely low dark current at 0 V bias,

 © 2021 Wiley-VCH GmbH

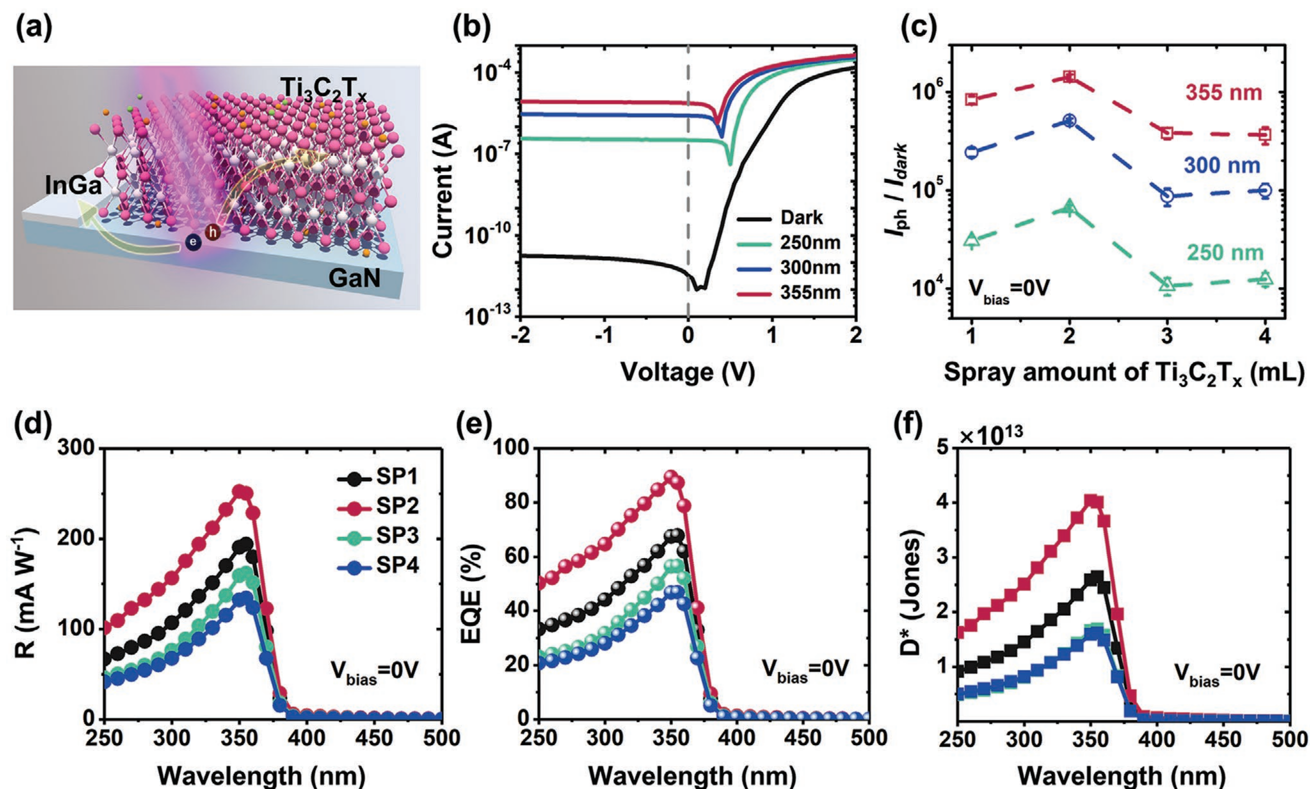

Figure 2. Photoelectric properties of the MXene/GaN photodiodes with different MXene thicknesses. a) Schematic diagram of the $Ti_3C_2T_x$ MXene/GaN photodiode. b) Typical *I–V* characteristics (in logarithmic scale) of the SP2 MXene/GaN vdWH photodiode under dark, 250, 300, and 350 nm UV light illumination, respectively; the light power densities for the measured wavelength of 250, 300, and 355 nm are 57, 344, and 662 µW cm^{-2} respectively. c) Variation of photo-to-dark current ratio I_{ph}/I_{dark} of the photodiode at 0 V bias versus spray amount of $Ti_3C_2T_x$. d) Spectral responsivity, e) EQE, and f) specific detectivity of the four photodiodes at 0 V bias.

which implies excellent recognition ability of light information from dark noises. The MXene film thickness dependent photoelectric characteristics are consistent with that of MXene/Si PDs.[29] Too thin the film may result in poor coverage and low sheet conductivity, while too thick the film will block UV light penetration (Figure 1i). A balanced conductivity and light absorption collectively contribute to the champion sample of SP2 device with prominent photoelectric properties. The time-dependent current curves of the SP1-SP4 photodiodes show high reproducibility and reversibility (see Figure S7, Supporting Information).

Spectral photodetection performances of the four photodiodes in the zero-bias mode are investigated, as shown in Figure 2d–f. The responsivity is defined as $R = I_{light}/(P_{in}S)$, where I_{light} is the net photocurrent, S is junction area of the vdWH devices (4 mm^2), P_{in} is the incident light power density. The EQE is the ratio of collected charge carriers to incident photons and is calculated by $EQE = I_{light}hc/(e\lambda P_{in})$, where parameters h, c, and λ are the Planck constant, the speed of light, and the wavelength of the incident light. The specific detectivity reflects weak light detection ability and is given by $D^* = R_\lambda/(2eI_{dark}/S)^{1/2}$ when the shot noise from the dark current is considered as the major contributor of background noise. The SP2 vdWH photodiode shows the best photoresponse performance. A peak responsivity of 252 mA W^{-1}, EQE of 89% and detectivity of 4.04×10^{13} Jones are obtained at 355 nm. As a comparison, Au/GaN Schottky photodiode shows much inferior response performance, with peak responsivity of 40 mA W^{-1}, EQE of 14% and detectivity of 9.54×10^{11} Jones (Figure S6, Supporting Information). In addition, the SP2 photodiode exhibits an reasonable UV/visible rejection ratio ($R_{355\ nm}/R_{500\ nm}$) of 532 (Figure S8, Supporting Information), since the absorption in the visible region of $Ti_3C_2T_x$ MXene.

The presented photodiode can also be operated in photovoltaic mode with self-bias circuit (Figure S9, Supporting Information). To investigate the photovoltaic response of the MXene/GaN vdWH photodiodes, power dependent photoresponse has been measured. As shown in **Figure 3**a, when the optical power density increasing from 30 to 720 µW cm^{-2}, the *I–V* curves shift upward successively under 355 nm light stimulation. The short-circuit current I_{sc} and open-circuit voltage V_{oc} are extracted from these curves. As shown in Figure 3b, the I_{sc} increases nearly linearly with illuminated optical power. By power fitting as $I_{sc} = AP^\theta$, it yields a θ value of 0.956, close to the unity, again indicating high-quality vdWH interface with few carrier traps.[40] The output electrical power P_{el}, which is usually used to describe the electricity generation capability of a photovoltaic detector or solar cell, is defined as $P_{el} = I_{light}V_{Bias}$.[41] The P_{el} as a function of V_{Bias} at the series of light power densities is displayed in Figure 3c. With the continuously upward-shifted *I–V* characteristics, the increased peak P_{el} with light power is understandable. Presented in Figure 3d, the gray rectangle area

© 2021 Wiley-VCH GmbH

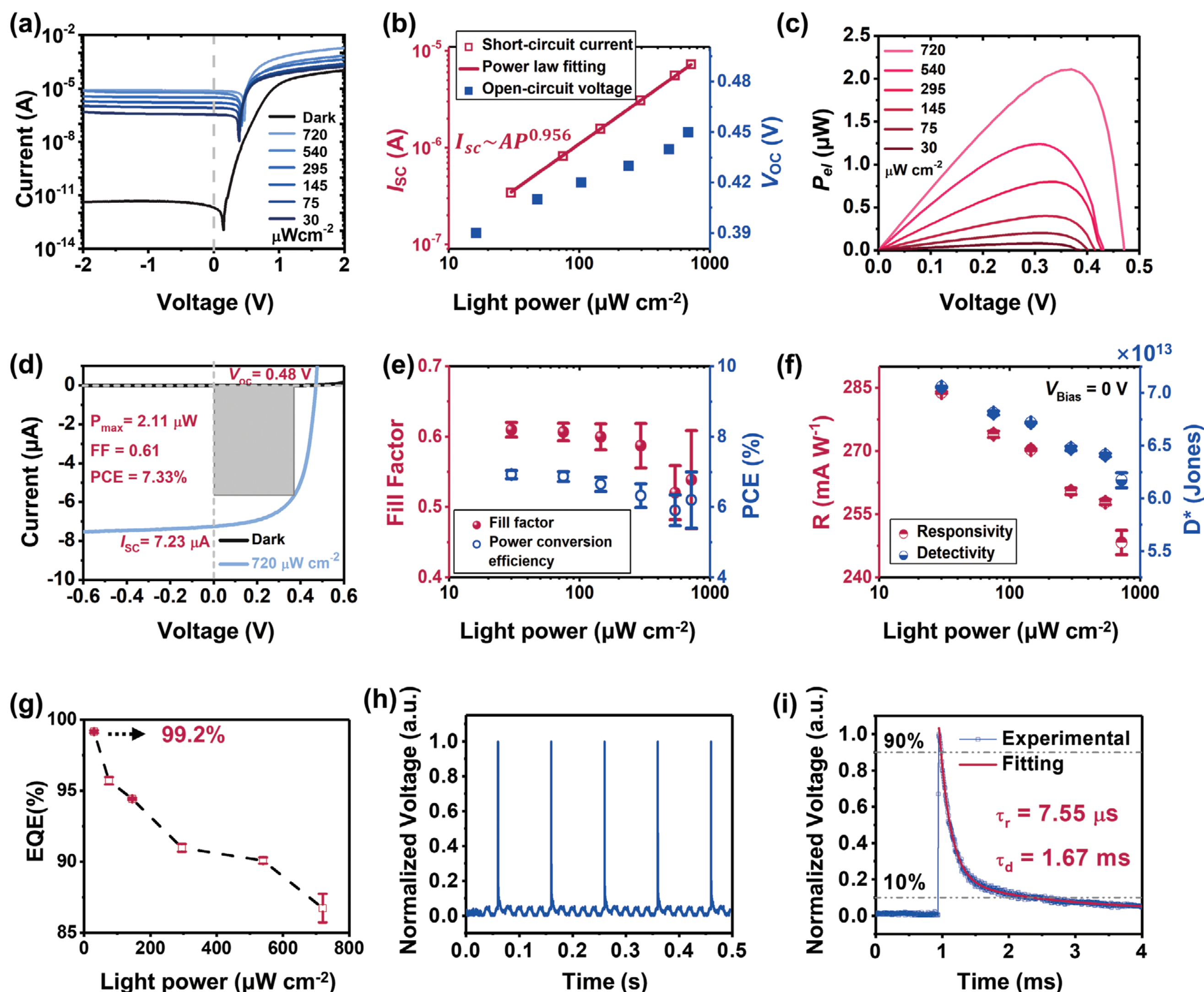

Figure 3. UV light (355 nm) power dependent a) *I–V* characteristics, b) short-circuit current I_{sc} and open-circuit voltage V_{oc} of the MXene/GaN Schottky photodiode. c) Output electrical power P_{el} as a function of bias voltage under different light (355 nm) power densities. d) *I–V* curves of the photodiode under dark (black curve) and 355 nm UV light illumination (light blue line) in linear scale. e–g) Light-power-dependent FF and PCE (e), responsivity and specific detectivity (f), and EQE (g) of the Schottky photodiode at 0 V bias. h,i) Response speed of the MXene/GaN to UV light. h) Typical pulse response of the photodiode to 355 nm pulse laser. i) A single pulse photoresponse extracted to evaluate the response speed, where the decay process is fitted with the second-order exponential fit.

marks the maximum output of electrical power P_{max}. The fill factor FF and PCE can be calculated by FF = $P_{max}/(I_{sc}V_{oc})$ and PCE = P_{max}/P_{in}, where P_{in} is the incident light power.[42] A typical P_{max} = 2.11 μW, FF = 0.61 and PCE = 7.33% are obtained under the 355 nm UV light with power density of 720 μW cm^{-2}, where high I_{sc} = 7.23 μA and V_{oc} = 0.48 V are achieved. Figure 3e displays the power dependent FF and PCE. Both FF and PCE show decreased trends when increasing optical power.

Further, we evaluate two important photodetection parameters, that is, responsivity and detectivity, of several SP2 vdWH photodiodes at 0 V bias under various light power densities. As presented in Figure 3f,g both responsivity and detectivity decline with the increase of light power density. At a low power density of 30 μW cm^{-2}, a superhigh responsivity of 284 mA W^{-1} and detectivity of 7.06 × 10^{13} Jones, along with a remarkable EQE of 99.2% are obtained. The excellent efficiency obtained in this work is the highest value, to the best of our knowledge, ever reported for a self-powered vdWH UV photodiode. Key performances of our device are compared with recently reported UV PDs, as listed in **Table 1**, indicating our device is highly competitive among self-powered UV PDs. It is worth noting that even at higher light power inputs, the EQE values are higher than 85% at the measured range, demonstrating robust self-powered UV photodetection capability. Moreover, considering the three orders of magnitudes' power density range experimented, the MXene/GaN vdWH photodiodes also exhibit good linear dynamic range, which is valuable for many practical applications.

The response speed is evaluated by a digital oscilloscope using a 355 nm pulse laser to stimulate the photodiode. Five fast-changing pulse responses are captured and exhibited in

© 2021 Wiley-VCH GmbH

Table 1. Key parameters of recently reported self-powered UV photodetectors, and a $Ti_3C_2T_x$-based UV photodetector is also listed for the comparison.

Devices	Wavelength [nm]	Self-powered	Responsivity [mA W^{-1}]	D^* [Jones]	EQE [%]	Rise/decay time	Ref.
$Ti_3C_2T_x$/GaN	355	Yes	284	7.06×10^{13}	99.2	7.55 µs/1.67 ms	This work
$PtSe_2$/GaN	265	Yes	193	3.8×10^{14}	90.3	45/102 µs	[18]
WS_2/GaN	375	Yes	226	4.0×10^{14}	74.7	7.3/420 µs	[20]
MoS_2/β-Ga_2O_3	245	Yes	2.05	1.21×10^{11}	10.4	–	[44]
Graphene/Si	365	Yes	200	1.6×10^{13}	68	4/12 ns	[39]
MoS_2/GaN	265	Yes	187	2.34×10^{13}	87.5	300/600 µs	[43]
2D $(BPA)_2PbBr_4$	377	Yes	≈0.1	≈10^7	2.8	27/30 µs	[45]
ZnO/$CuCrO_2$	365	Yes	3.43	8.5×10^9	1.2	32/35 µs	[46]
Perovskite–CuO	350	Yes	126.3	3.97×10^{12}	44.7	<200/200 ms	[47]
Ag/BFO/ITO	365	Yes	2.23	5.13×10^7	0.76	–	[48]
Mesoporous TiO_2/Spiro-OMeTAD	380	Yes	64	–	20.9	<3 ms	[49]
Au/TiO_2/P3HT	350	Yes	0.25	1.09×10^{10}	0.09	0.48/2.12 s	[50]
Perovskite/Spiro-OMeTAD	254	Yes	52.68	4.65×10^{11}	25.7	46/47 ms	[51]
$Ti_3C_2T_x$/TiO_2	350	No (5V)	6.0	≈10^{11}	21.3	2.27/2.54 s	[30]

Figure 3h. A single pulse is magnified to evaluate the rise and decay time, as displayed in Figure 3i and Figure S10, Supporting information. The rise time is estimated by the time taken from 10% to 90% of the maximum photocurrent, whereas to better assess the decay process, a second-order exponential fit is applied. The MXene/GaN vdWH photodiode displays a fast response to the UV light with rise time $\tau_r = 7.55$ µs and decay time $\tau_d = 1.67$ ms, which is comparable to most UV PDs listed in Table 1.

Next, a promising interpretation for the underlying mechanism for the ultrahigh-efficiency photovoltaic UV photodiode is proposed. To disclose the electronic structures of the MXene/GaN vdWH diode, the WF of the as-synthesized $Ti_3C_2T_x$ MXene was calculated from SKPFM measurements. **Figure 4**a shows the SKPFM mapping of MXene on GaN. The surface potential along the marked dash line is presented in Figure 4b, where a surface potential difference of ≈0.90 eV was obtained between $Ti_3C_2T_x$ and GaN. The Fermi level of GaN can be readily estimated to be 4.22 eV by $E_{(C,GaN)} - E_{(F,GaN)} = K_B T \ln(N_C/N_d)$ with $N_C = 2.3 \times 10^{18}$ cm^{-3} for wurtzite GaN[52] and $N_d = 2.7 \times 10^{16}$ cm^{-3} determined from Hall measurements. In this scenario, the WF of the as-synthesized $Ti_3C_2T_x$ was estimated to be 5.10 eV. The obtained WF is slightly higher than the reported value of 4.98 eV[53] but lower than the spin coated MXene film of 5.28 eV,[54] which may have close relationship with the –OH, –O, and –F surface terminations of $Ti_3C_2T_x$ MXene.[28] Thus, the energy band diagram of the MXene/GaN vdWH diode can be plotted, as illustrated in Figure 4c. It reveals a sharp band bending at the junction interface due to the large WF difference, forming a strong built-in electric field pointing from GaN to $Ti_3C_2T_x$. The depletion region width was determined to be ≈187 nm at 0 V bias (Note S1, Supporting information). When the device is under UV beam illumination, although a part of UV photons are absorbed by the MXene, most of them can penetrate through the MXene and reach at the depletion region within GaN side, considering a penetration depth of ≈106 nm for GaN with absorption coefficient ≈9.43×10^4 cm^{-1}.[55] Subsequently, photogenerated electron/hole pairs within the depletion region are promptly and effectively separated by the built-in electric field to form photocurrent, leading to the highly efficienct UV light response.

Moreover, I–V curves in the dark of six SP2 MXene/GaN vdWH diodes were fitted (see Note S2, Figures S11 and S12, Supporting Information) by the thermionic emission mode using Chung's method,[56] which yields Schottky barrier heights in the range of 0.95–1.03 eV. A typical fitted curve is presented in Figure 4d. The derived Schottky barrier height of 1.02 eV agrees well with the calculated value of 1.0 eV based on the SKPFM results, as discussed above. Moreover, the vdWH photodiode presents a surprisingly high EQE value close to the unity at wavelength of 355 nm (30 µW cm^{-2}) under 0 V bias. This may be attributed to the dominated interband transition absorption of MXene in UV region that induces photoexcited hot carriers crossing the Schottky barrier after different thermal relaxation processes,[57] which are collected by the electrode after drifting through the depletion layer under the strong built-in electric field (schematically demonstrated in Figure 4c). The observed effect is in consistent with that of graphene/Si ultra-shallow junction photodiode.[39] Hence, the two important factors, strong built-in electric field for effectively separating photoinduced electron/hole pairs and additional contribution of hot photocarriers, play synergistic effects on the resulted superhigh quantum efficiency.

Spray optoelectronics is an attractive technique with several advantages, such as large-scale production, simple processing, and low cost, etc.[58] To verify the feasibility and reliablity, MXene/GaN vdWH photodiode arrays were fabricated. The photodiode arrays were fabricated with two different contact areas (2 and 4 mm^2) by controlling the masks, as shown in **Figure 5**a,d. Heat maps in Figure 5b,c, respectively, show dark current and photocurrent for 3×5 photodiode arrays with junction area of 2 mm^2, which reveals uniform current distribution with dark current in the range of 1.2–2.1 pA and photocurrent varying from 3.0 to 3.9 µA. Heat maps of dark current and photocurrent with junction area of 4 mm^2 (Figure 5e,f,

© 2021 Wiley-VCH GmbH

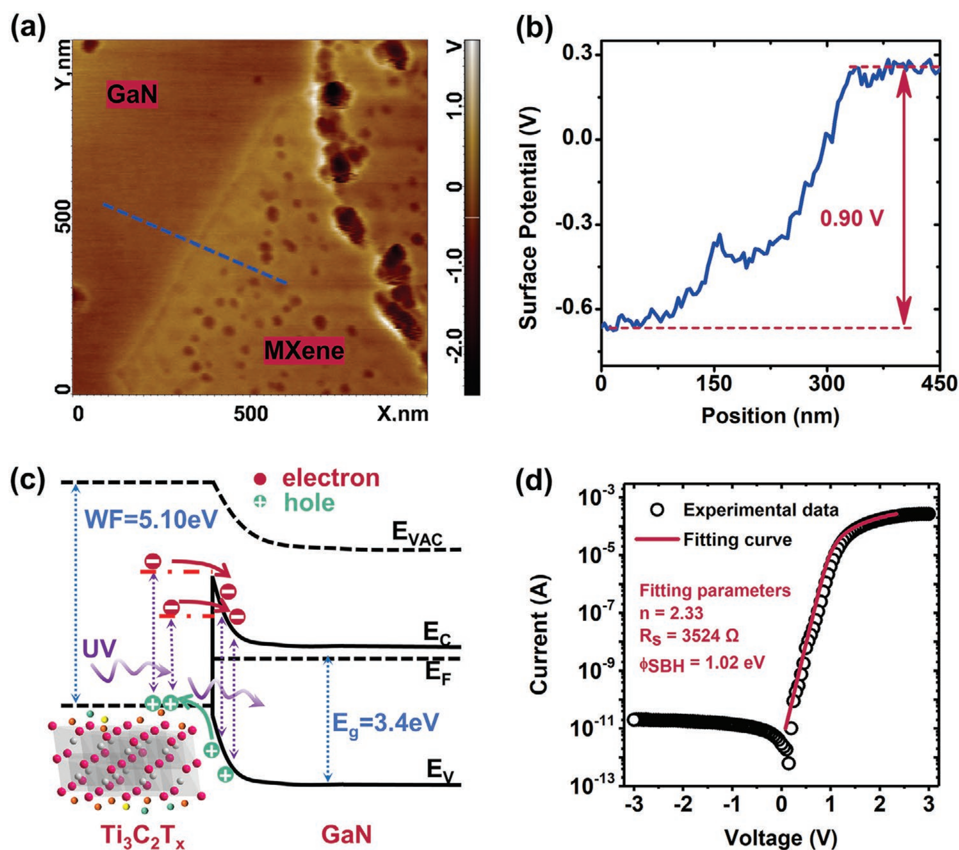

Figure 4. Electronic structure and energy band relationship of $Ti_3C_2T_x$/GaN vdWH. a) SKPFM mapping of $Ti_3C_2T_x$/GaN and b) surface potential along the dashed line marked in (a). c) Proposed energy band diagram of $Ti_3C_2T_x$/GaN heterojunction based on SKPFM calculation. d) Typical dark *I–V* and corresponding fitting curves of the $Ti_3C_2T_x$/GaN vdWH, where fitting parameters are given.

respectively) exhibit very low dark current (in pA magnitude) with small fluctuations, whereas their photocurrent distribution is relatively uniform, with values in the range of 7.0–8.0 µA. The highly homogenous and reliable cell-to-cell performances indicate that the spray deposited $Ti_3C_2T_x$ MXene/GaN vdWH photodiode arrays are applicable toward large-scale production.

3. Conclusion

Self-powered and high-performance MXene/GaN vdWH UV photodiodes are successfully fabricated through a simple and low-cost spray-deposition route. It is found that such integration forms sufficient and robust Schottky-junction-induced built-in electric field to separate photocarriers. The $Ti_3C_2T_x$ MXene absorption in UV range produces photoexcited hot carriers crossing the energy barrier, generating additional photocurrent, leading to an ultrahigh IQE over 100% and EQE over 99%. As a result, the proposed UV photodiodes exhibit remarkable photoresponse performances in self-powered mode, such as a large responsivity of 284 mA W^{-1}, a surprising EQE of 99.2%, a high specific detectivity of 7.06 × 10^{13} Jones and fast response speed (rise/decay time of 7.55 µs/1.67 ms) under 355 nm UV illumination (30 µW cm^{-2}). Furthermore, the photovoltaic behavior is assessed, giving a reasonable PCE of 7.33%. The additional device array prototypes with uniform and stable photocurrent outputs ability demonstrate high prospect for practical applications.

4. Experimental Section

Materials Preparation: The unintentionally-doped GaN (4–5 µm, $N_d = 2.7 \times 10^{16}$ cm^{-3} by Hall measurements) wafer on sapphire substrate was epitaxial grown by using a metal–organic chemical vapor deposition system. The few-layered $Ti_3C_2T_x$ colloidal solution (5 mg mL^{-1}) was purchased from Jilin 11 Technology Co., Ltd., which was obtained through the minimally intensive layer delamination method from Ti_3AlC_2. The purchased solution was washed via a centrifugation (3500 rpm, 20 min) process in ice water, then the supernatant was decanted into waste, followed by the addition of deionized (DI) water and hand-shaking for 5 min. The above washing process was repeated for several times. The final product was diluted using DI water with volume ratio of 1:15, allowing for the following device fabrication. To protect the as-obtained $Ti_3C_2T_x$ from potential oxidation, it was stored in a refrigerator with vacuum seal, ready for use.

Device Fabrication: The GaN wafer was cut into small pieces and was washed using acetone, ethanol, DI water, and diluted HCl in sequence. Before MXene spray coating, the GaN piece was immersed in piranha solution for several minutes for surface hydrophilic treatment and then it was blow-dried by N_2 for next procedure. Warning: the piranha solution consists of a 3:1 mixture of concentrated sulfuric acid with 30% hydrogen peroxide, which is a strong oxidizing agent that should be handled with extremely careful precautions. The as-obtained $Ti_3C_2T_x$ colloidal suspension was then sprayed onto a piece of GaN placed on

© 2021 Wiley-VCH GmbH

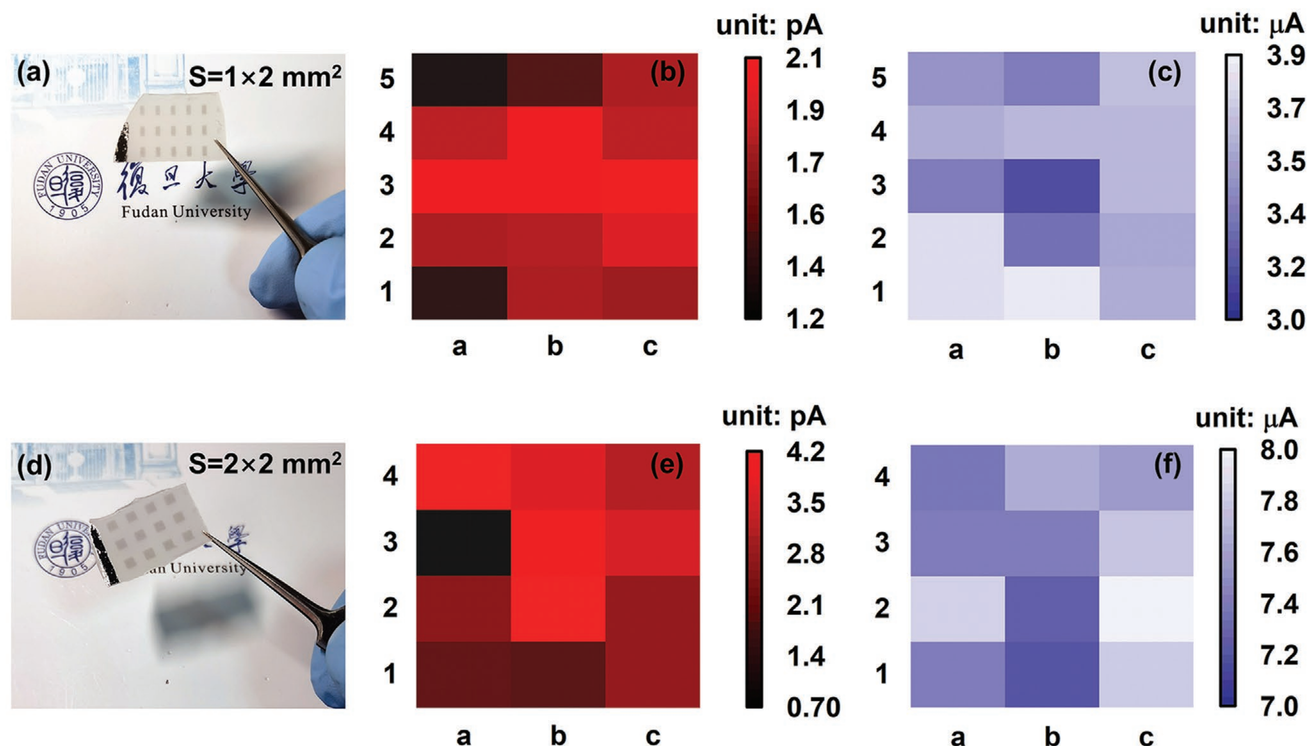

Figure 5. Heat maps of photocurrent and dark current for the MXene/GaN vdWH photodiode arrays with different junction areas at 0 V bias. a–f) Digital image, dark current, and photocurrent of electrode area of 1 × 2 mm^2 (a–c) and 2 × 2 mm^2 (d–f), respectively.

a hot plate (80 °C) with a shadow mask using a spray gun. The spray amount of few-layered $Ti_3C_2T_x$ solutions were controlled (1, 2, 3, 4 mL, denoted as SP1, SP2, SP3, SP4 respectively) while keeping a constant spray flow rate to acquire different $Ti_3C_2T_x$ nanosheet film thickness. After the deposition, the $Ti_3C_2T_x$/GaN sample was moved to a N_2 glovebox overnight for further dry. Finally, InGa eutectic was casted on GaN side for ohmic contact, while a small drop of Ag paste was dropped onto a corner of the $Ti_3C_2T_x$ and dried for photoelectrical measurements.

Characterization and Measurements: The sample morphologies were characterized by a field-emission scanning electron microscope (Zeiss Sigma). XRD patterns were conducted on a Bruker D8 diffractometer equipped with Cu Kα radiation (λ = 1.5405 Å). Raman spectra were collected by using a micro-Raman spectrometer (LabRAM HR UV-NIR, Horiba). The transmittance/absorption spectra were experimented on an UV–vis spectrometer (Hitachi U-3900H). The surface potential difference was collected by an atomic force microscope (NT-MDT). The optoelectronic properties were conducted on a PD characterization system which consists of a semiconductor parameter analyzer (Keithley 4200-SCS) and a 70 W xenon arc lamp in combination with a monochromator as light sources. During the tests, the MXene electrode acted as an anode, while the InGa Ohmic contact acted as a cathode. A Nova II power meter (OPHIR photonics) was used to calibrate the light power. The response speed of MXene/GaN vdWH photodiodes was evaluated by connecting the photodiode with a 1GΩ resistor while a 355 nm Nd:YAG pulsed laser and a digital oscilloscope (Tektronix DPO 5140B) were used as light stimuli and data collection respectively. All these measurements were conducted under ambient conditions at room temperature.

Supporting Information

Supporting Information is available from the Wiley Online Library or from the author.

Acknowledgements

This work was supported by National Key R&D Program of China (No. 2018YFA0703700 and 2017YFA0204600), Key Field R&D Program in Guangdong Province (2020B010174004), Featured Innovation Projects of Colleges and Universities in Guangdong Province (2018KTSCX232), Guangdong Basic and Applied Basic Research Foundation (2020A1515110185), Key Laboratory of Optoelectronic materials and Applications in Guangdong Higher Education (2017KSYS011).

Conflict of Interest

The authors declare no conflict of interest.

Data Availability Statement

The data that support the findings of this study are available from the corresponding author upon reasonable request.

Keywords

MXene/GaN, self-powered devices, ultraviolet photodiodes, van der Waals heterojunctions

Received: February 7, 2021
Revised: April 1, 2021
Published online:

© 2021 Wiley-VCH GmbH

[1] J. Yao, G. Yang, *Nanoscale* **2020**, *12*, 454.
[2] X. Xu, J. Chen, S. Cai, Z. Long, Y. Zhang, L. Su, S. He, C. Tang, P. Liu, H. Peng, X. S. Fang, *Adv. Mater.* **2018**, *30*, 1803165.
[3] Y. Lu, J. Chen, T. X. Chen, Y. Shu, R. Chang, Y. Sheng, V. Shautsova, N. Mkhize, P. Holdway, H. Bhaskaran, J. H. Warner, *Adv. Mater.* **2020**, *32*, 1906958.
[4] L. Su, W. Yang, J. Cai, H. Chen, X. S. Fang, *Small* **2017**, *13*, 1701687.
[5] Y. Wang, K. Ding, B. Sun, S.-T. Lee, J. Jie, *Nano Res.* **2016**, *9*, 72.
[6] H. P. Wang, S. Y. Li, X. Y. Liu, Z. F. Shi, X. S. Fang, J. H. He, *Adv. Mater.* **2021**, *33*, 2003309.
[7] M. Long, P. Wang, H. Fang, W. Hu, *Adv. Funct. Mater.* **2018**, *29*, 1803807.
[8] F. Wang, T. Gao, Q. Zhang, Z. Y. Hu, B. Jin, L. Li, X. Zhou, H. Li, G. Van Tendeloo, T. Zhai, *Adv. Mater.* **2019**, *31*, 1806306.
[9] J. Chu, F. Wang, L. Yin, L. Lei, C. Yan, F. Wang, Y. Wen, Z. Wang, C. Jiang, L. Feng, J. Xiong, Y. Li, J. He, *Adv. Funct. Mater.* **2017**, *27*, 1701342.
[10] C. Gong, J. Chu, S. Qian, C. Yin, X. Hu, H. Wang, Y. Wang, X. Ding, S. Jiang, A. Li, Y. Gong, X. Wang, C. Li, T. Zhai, J. Xiong, *Adv. Mater.* **2020**, *32*, 1903580.
[11] W. Zeng, J. Li, L. Feng, H. Pan, X. Zhang, H. Sun, Z. Liu, *Adv. Funct. Mater.* **2019**, *29*, 1900129.
[12] S. Li, Y. Zhang, W. Yang, H. Liu, X. S. Fang, *Adv. Mater.* **2020**, *32*, 1905443.
[13] Z. Zhang, P. Lin, Q. Liao, Z. Kang, H. Si, Y. Zhang, *Adv. Mater.* **2019**, *31*, 1806411.
[14] D. Jariwala, T. J. Marks, M. C. Hersam, *Nat. Mater.* **2017**, *16*, 170.
[15] Z. Lu, Y. Xu, Y. Yu, K. Xu, J. Mao, G. Xu, Y. Ma, D. Wu, J. Jie, *Adv. Funct. Mater.* **2020**, *30*, 1907951.
[16] W. Chen, R. Liang, S. Zhang, Y. Liu, W. Cheng, C. Sun, J. Xu, *Nano Res.* **2019**, *13*, 127.
[17] K. Montazeri, M. Currie, L. Verger, P. Dianat, M. W. Barsoum, B. Nabet, *Adv. Mater.* **2019**, *31*, 1903271.
[18] R. Zhuo, L. Zeng, H. Yuan, D. Wu, Y. Wang, Z. Shi, T. Xu, Y. Tian, X. Li, Y. H. Tsang, *Nano Res.* **2018**, *12*, 183.
[19] S. H. Bae, H. Kum, W. Kong, Y. Kim, C. Choi, B. Lee, P. Lin, Y. Park, J. Kim, *Nat. Mater.* **2019**, *18*, 550.
[20] Z. Zhao, D. Wu, J. Guo, E. Wu, C. Jia, Z. Shi, Y. Tian, X. Li, Y. Tian, *J. Mater. Chem. C* **2019**, *7*, 12121.
[21] Z. Wang, H. Kim, H. N. Alshareef, *Adv. Mater.* **2018**, *30*, 1706656.
[22] C. J. Zhang, B. Anasori, A. Seral-Ascaso, S. H. Park, N. McEvoy, A. Shmeliov, G. S. Duesberg, J. N. Coleman, Y. Gogotsi, V. Nicolosi, *Adv. Mater.* **2017**, *29*, 1702678.
[23] H. C. Fu, V. Ramalingam, H. Kim, C. H. Lin, X. S. Fang, H. N. Alshareef, J. H. He, *Adv. Energy Mater.* **2019**, *9*, 1900180.
[24] S. Ahn, T. H. Han, K. Maleski, J. Song, Y. H. Kim, M. H. Park, H. Zhou, S. Yoo, Y. Gogotsi, T. W. Lee, *Adv. Mater.* **2020**, *32*, 2000919.
[25] W. X. Ouyang, J. X. Chen, J. H. He, X. S. Fang, *Adv. Electron. Mater.* **2020**, *6*, 2000168.
[26] M. Naguib, M. Kurtoglu, V. Presser, J. Lu, J. Niu, M. Heon, L. Hultman, Y. Gogotsi, M. W. Barsoum, *Adv. Mater.* **2011**, *23*, 4248.
[27] P. Perumal, C. Karuppiah, W. C. Liao, Y. R. Liou, Y. M. Liao, Y. F. Chen, *Sci. Rep.* **2017**, *7*, 10002.
[28] Y. Liu, H. Xiao, W. A. Goddard, 3rd, *J. Am. Chem. Soc.* **2016**, *138*, 15853.
[29] Z. Kang, Y. Ma, X. Tan, M. Zhu, Z. Zheng, N. Liu, L. Li, Z. Zou, X. Jiang, T. Zhai, Y. Gao, *Adv. Electron. Mater.* **2017**, *3*, 1700165.
[30] J. Chen, Z. Li, F. Ni, W. Ouyang, X. S. Fang, *Mater. Horiz.* **2020**, *7*, 1828.
[31] W. Deng, H. Huang, H. Jin, W. Li, X. Chu, D. Xiong, W. Yan, F. Chun, M. Xie, C. Luo, L. Jin, C. Liu, H. Zhang, W. Deng, W. Yang, *Adv. Opt. Mater.* **2019**, *7*, 1801521.
[32] Y. M. Sun, W. D. Song, F. L. Gao, X. F. Wang, X. J. Luo, J. Q. Guo, B. L. Zhang, J. Shi, C. Chen, Q. Liu, S. T. Li, *ACS Appl. Mater. Interfaces* **2020**, *12*, 13473.
[33] W. D. Song, X. F Wang, C. Xia, R. P. Wang, L. L. Zhao, D. X. Guo, H. Chen, J. K. Xiao, S. C. Su, S. T. Li, *Nano Energy* **2017**, *33*, 272.
[34] W. D. Song, X. F. Wang, H. Chen, D. X. Guo, M. Y. Qing, W. X. Hu, X. J. Luo, X. Luo, G. Li, S. T. Luo, *J. Mater. Chem. C* **2017**, *5*, 11551.
[35] W. Tian, A. VahidMohammadi, Z. Wang, L. Ouyang, M. Beidaghi, M. M. Hamedi, *Nat. Commun.* **2019**, *10*, 2558.
[36] B. Anasori, M. R. Lukatskaya, Y. Gogotsi, *Nat. Rev. Mater.* **2017**, *2*, 16098.
[37] J. Luo, W. Zhang, H. Yuan, C. Jin, L. Zhang, H. Huang, C. Liang, Y. Xia, J. Zhang, Y. Gan, X. Tao, *ACS Nano* **2017**, *11*, 2459.
[38] L. Zheng, W. Hu, X. Shu, H. Zheng, X. S. Fang, *Adv. Mater. Interfaces* **2018**, *5*, 1800515.
[39] X. Wan, Y. Xu, H. Guo, K. Shehzad, A. Ali, Y. Liu, J. Yang, D. Dai, C.-T. Lin, L. Liu, H.-C. Cheng, F. Wang, X. Wang, H. Lu, W. Hu, X. Pi, Y. Dan, J. Luo, T. Hasan, X. Duan, X. Li, J. Xu, D. Yang, T. Ren, B. Yu, *npj 2D Mater. Appl.* **2017**, *1*, 4.
[40] W. Ouyang, F. Teng, X. S. Fang, *Adv. Funct. Mater.* **2018**, *28*, 1707178.
[41] L. Wang, L. Huang, W. C. Tan, X. Feng, L. Chen, X. Huang, K.-W. Ang, *Small Methods* **2018**, *2*, 1700294.
[42] C. Li, Q. Cao, F. Wang, Y. Xiao, Y. Li, J.-J. Delaunay, H. Zhu, *Chem. Soc. Rev.* **2018**, *47*, 4981.
[43] R. Zhuo, Y. Wang, D. Wu, Z. Lou, Z. Shi, T. Xu, J. Xu, Y. Tian, X. Li, *J. Mater. Chem. C* **2018**, *6*, 299.
[44] R. Zhuo, D. Wu, Y. Wang, E. Wu, C. Jia, Z. Shi, T. Xu, Y. Tian, X. Li, *J. Mater. Chem. C* **2018**, *6*, 10982.
[45] C. Ji, D. Dey, Y. Peng, X. Liu, L. Li, J. Luo, *Angew. Chem. Int., Ed. Engl.* **2020**, *59*, 18933.
[46] T. Cossuet, J. Resende, L. Rapenne, O. Chaix-Pluchery, C. Jiménez, G. Renou, A. J. Pearson, R. L. Z. Hoye, D. Blanc-Pelissier, N. D. Nguyen, E. Appert, D. Muñoz-Rojas, V. Consonni, J.-L. Deschanvres, *Adv. Funct. Mater.* **2018**, *28*, 1803142.
[47] H. Sun, W. Tian, F. Cao, J. Xiong, L. Li, *Adv. Mater.* **2018**, *30*, 1706986.
[48] R. Zhao, N. Ma, K. Song, Y. Yang, *Adv. Funct. Mater.* **2019**, *30*, 1906232.
[49] T. Zhu, J. Su, J. Alvarez, G. Lefèvre, F. Labat, I. Ciofini, T. Pauporté, *Adv. Funct. Mater.* **2019**, *29*, 1903981.
[50] L. Zheng, X. Deng, Y. Wang, J. Chen, X. S. Fang, L. Wang, X. Shi, H. Zheng, *Adv. Funct. Mater.* **2020**, *30*, 2001604.
[51] T. M. H. Nguyen, S. Kim, C. W. Bark, *J. Mater. Chem. A* **2021**, *9*, 1269.
[52] H. Chandrasekar, M. Singh, S. Raghavan, N. Bhat, *Semicond. Sci. Technol.* **2015**, *30*, 115018.
[53] J. Xu, J. Shim, J.-H. Park, S. Lee, *Adv. Funct. Mater.* **2016**, *26*, 5328.
[54] M. Mariano, O. Mashtalir, F. Q. Antonio, W. H. Ryu, B. Deng, F. Xia, Y. Gogotsi, A. D. Taylor, *Nanoscale* **2016**, *8*, 16371.
[55] J. F. Muth, J. H. Lee, I. K. Shmagin, R. M. Kolbas, H. C. Casey, B. P. Keller, U. K. Mishra, S. P. DenBaars, *Appl. Phys. Lett.* **1997**, *71*, 2572.
[56] S. K. Cheung, N. W. Cheung, *Appl. Phys. Lett.* **1986**, *49*, 85.
[57] D. B. Velusamy, J. K. El-Demellawi, A. M. El-Zohry, A. Giugni, S. Lopatin, M. N. Hedhili, A. E. Mansour, E. D. Fabrizio, O. F. Mohammed, H. N. Alshareef, *Adv. Mater.* **2019**, *31*, 1807658.
[58] J. Yuan, C. Bi, S. Wang, R. Guo, T. Shen, L. Zhang, J. Tian, *Adv. Funct. Mater.* **2019**, *29*, 1970337.

© 2021 Wiley-VCH GmbH